POLISH POLAR RESEARCH
vol. 34, no. 2, pp. 111–138, 2013 doi: 10.2478/popore-2013-0011

Seismic and density structure of the lithosphere-asthenosphere system along transect Knipovich Ridge-Spitsbergen-Barents Sea – geological and petrophysical implications

Lech KRYSIŃSKI [1], Marek GRAD [2]*, Rolf MJELDE [3], Wojciech CZUBA [4] and Aleksander GUTERCH [4]

[1] *Instytut Badawczy Dróg i Mostów, ul. Instytutowa 1, 03-302 Warszawa, Poland <lkrys@mimuw.edu.pl>*

[2] *Instytut Geofizyki, Wydział Fizyki, Uniwersytet Warszawski, ul. Pasteura 7, 02-093 Warszawa, Poland <mgrad@mimuw.edu.pl>*

[3] *Department of Earth Science, University of Bergen, Allegaten 41, N-5020 Bergen, Norway <Rolf.Mjelde@geo.uib.no>*

[4] *Instytut Geofizyki, Polska Akademia Nauk, ul. Ks. Janusza 64, 01-452 Warszawa, Poland <wojt@igf.edu.pl, aguterch@igf.edu.pl>*

* *corresponding author*

Abstract: This paper presents a study of the seismic P-wave velocity and density structure of the lithosphere-asthenosphere system along a 800 km long transect extending from the actively spreading Knipovich Ridge, across southern Spitsbergen to the Kong Karls Land Volcanic Province. The 2D seismic and density model documents 6–8 km thick oceanic crust formed at the Knipovich Ridge, a distinct continent-ocean-boundary (COB), the eastern boundary of the dominantly sheared Hornsund Fault Zone, and the eastern boundary of the Early Cenozoic West Spitsbergen Fold-and-Thrust Belt. The crustal continent-ocean transitional zone has significant excess of density (more than 0.1 g/cm^3 in average), characteristic for mafic/ultramafic and high-grade metamorphic rocks. The main Caledonian suture zone between Laurentia and Barentsia is interpreted based on variations in crustal thickness, velocities and densities. A high velocity body in the lower crust is preferably interpreted in terms of Early Cretaceous magmatism channelled from an Arctic source southwards along the proto-Hornsund zone of weakness. The continental upper mantle expresses high velocities (8.24 km/s) and densities (3.2 g/cm^3), which may be interpreted in terms of low heat-flow and composition dominated by dunites. The lower velocities (7.85 km/s) and densities (3.1 g/cm^3) observed in the oceanic lithosphere suggest composition dominated by primitive peridotites. The model of mantle allows for successful direct description of subcrustal masses distribution compensating isostatically uneven crustal load. The estimated low value of correlation between density and velocity in the mantle 0.12 kg·s·m^{-4} suggests that horizontal density differences between oceanic and continental mantle would be dominated by compositional changes.

Key words: Arctic, crust, LAB – lithosphere-asthenosphere boundary, gravity modelling, mantle composition.

Introduction

The development of the North Atlantic rifting and subsequent sea-floor spreading together with development of the passive sheared continental margin of the Barents Sea continental platform are processes which form the present day face of our planet. The development of this margin is strongly connected to the history of rifting and subsequent sea-floor spreading in the North Atlantic Ocean (Jackson *et al.* 1990; Lyberis and Manby 1993a, b; Ohta 1994).

In this paper we present an 800 km long transect crossing the Knipovich Ridge in the Northern Atlantic, the continent-ocean boundary (COB), southern Spitsbergen along Hornsund, Storfjorden and Edgeøya, and the western Barents Sea continental platform (Fig. 1). Previously this region has been studied by geophysical surveys, including active and passive seismic experiments, gravity and magnetic (*e.g.* Vogt *et al.* 1979; Taylor *et al.* 1981; Sellevoll 1982; Davydova *et al.* 1985; Faleide *et al.* 1991; Klingelhöfer *et al.* 2000a, b; Mjelde *et al.* 2002; Breivik *et al.* 2003; Ljones *et al.* 2004; Czuba *et al.* 2008). Most of the study area around Spitsbergen and in the Barents Sea has a water depth about 250 m only (Fig. 2). In the west, the water depth is increasing to about 2000–2500 m. The deepest parts are located in the rift valley of the actively spreading Knipovich Ridge (about 3000 m) and the Molloy Deep (about 4000 m). Magnetic anomalies are mostly from -100 to +50 nT (Fig. 3). Positive anomalies over +150 nT are observed west of Hornsund (76.8°N, 13.0°E), south of Sørkapp (75.0°N, 19.0°E) and in the Barents Sea west of Edgeøya (77.2°N, 27.5°E). They have all circular or elliptic shape with 50 to 100 km diameter. Another group of smaller anomalies occurs in the area of Kong Karls Land.

The gravity map of the study area (Fig. 4) is compiled from free-air anomalies at the sea and Bouguer anomaly on the land with a correction for density of 2.67 g/cm^3. In the oceanic part of the area the gravity anomalies are from +20 to +60 mGal, with exception of a band of 0 mGal values along the central part of Knipovich Ridge. Anomalies larger than 100 mGal are observed along the COB, approximately from 75°N to 76°N. Southern Spitsbergen is characterized by an anomaly about -50 mGal, and the western Barents Sea show values of about -20 to +20 mGal.

The study area is unique in the sense that the transect covers the remnants of the Caledonian mountain range, *c.* 300 Ma of extensional and magmatic processes culminating at continental break-up along a very narrow sheared margin, and very thin oceanic crust formed along the ultra-slow spreading Knipovich Ridge. Our main aim is to provide new constraint on some of these processes by focusing on gravity modelling for the crust and uppermost mantle.

Tectonic setting

The assembly of the crystalline basement of the western Barents Sea is to a large extent related to the Caledonian orogeny (*e.g.* Doré 1991). Baltica and

Laurentia collided in Silurian time, followed by several rifting events starting in Late Paleozoic time. As the rifting stopped, the Barents Shelf gently subsided as it cooled, and a carbonate platform developed (Worsley 2008). In Triassic, the sedimentation pattern changed towards siliciclastic rocks, deposited from the east and southeast (Riis *et al.* 2008). The second phase of rifting occurred in the Late Jurassic–Early Cretaceous as a response to the northward propagation of the Atlantic (Faleide *et al.* 2008).

The continental breakup occurring at the Paleocene–Eocene transition was accompanied by voluminous magmatism on the Norwegian and East Greenland margins (Eldholm *et al.* 2002). The western Barents Sea margin developed in a dominantly shear environment with only minor magmatic activity, with the exception of the Vestbakken Volcanic Province (Faleide *et al.* 1993).

Cenozoic tectonic processes in the Svalbard region were closely related to the structural history of the western Barents Sea margin. The relative motion between Svalbard and Greenland took place along the NNW-SSE trending Hornsund Fault Zone. This regional fault zone acted as an incipient plate boundary between the Barents Sea shelf and the emerging Arctic Ocean. No significant separation between Svalbard and Greenland occurred until about 36 Ma ago, when the relative plate motion between Greenland and Eurasia changed and induced an extensional component along the initially sheared segments. Late Cenozoic uplift and erosion has removed most of the Paleogene and Cretaceous succession in the northwestern Barents Sea (Faleide *et al.* 1996). The spreading axis in the Greenland Sea is today represented by the Knipovich Ridge (Fig. 1). The Hornsund Fault, the prominent tectonic structure which parallels the Knipovich Ridge to the east, can be traced from just south of Bjørnøya at *c.* 75°N to about 79°N (Sundvor and Eldholm 1979, 1980).

Seismic model

The seismic crustal model along the transect was compiled from refraction profiles performed in this area: Profile 8 (Ljones *et al.* 2004), profile Horsted'05 (Czuba *et al.* 2008), Profile KKL (Minakov *et al.* 2012) and a 3D crustal model of the Barents Sea (Levshin *et al.* 2007; Ritzmann *et al.* 2007). The location map of the seismic transect in southern Spitsbergen, between the Knipovich Ridge and the Barents Sea is shown in Fig. 1 (highlighted by grey bar). For Profile 8 green filled triangles are OBSs numbered from 1 to 10, and green dots are airgun shots with average distance interval 200 m. For profile Horsted'05 red filled triangles are OBSs and land stations (obs and spi, from 11 to 31), red stars are chemical shots, and red dots are airgun shots with average distance interval 800 m. For Profile KKL blue dots are airgun shots with average distance interval 200 m and blue filed circles are OBSs. Big blue pentagons show the location of crustal data from the 3D model of the Barents Sea. Geographical coordinates of

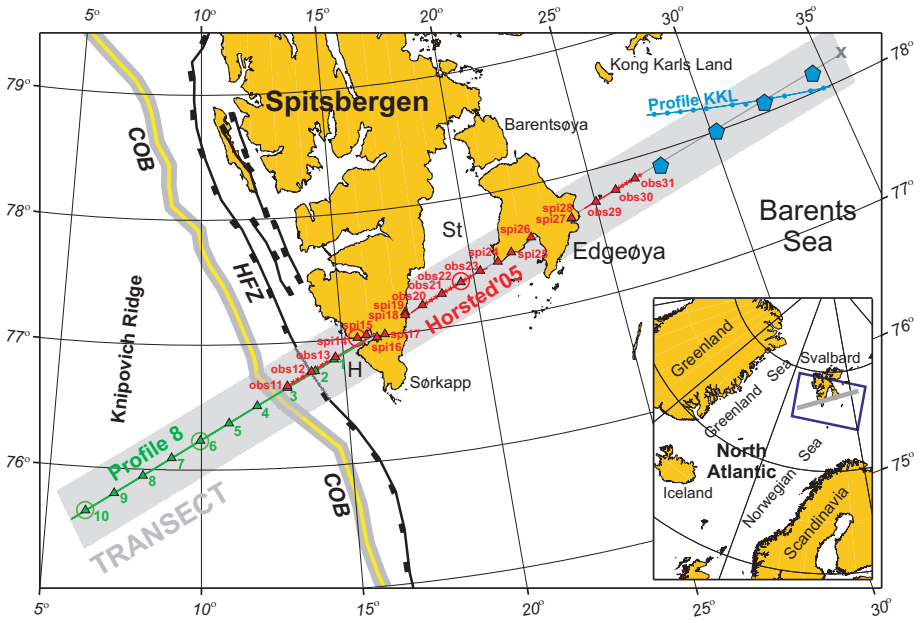

Fig. 1. Location map of the seismic transect in southern Spitsbergen, between the Knipovich Ridge and the Barents Sea (highlighted by grey bar). COB – continent-ocean boundary (Breivik *et al.* 1999); H – Hornsund; HFZ – Hornsund Fault Zone; St – Storfjorden. See text for more explanations.

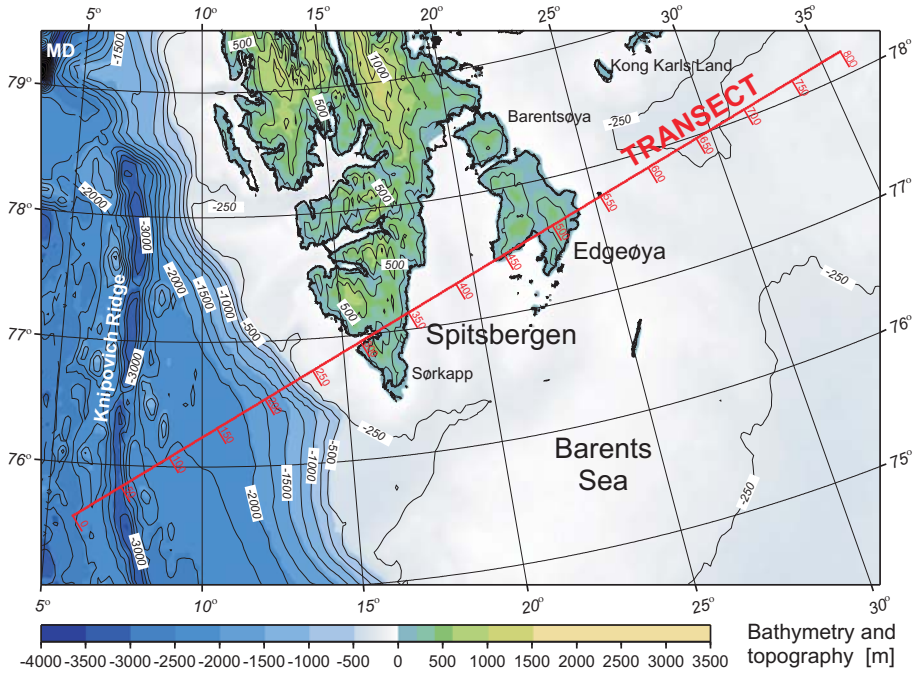

Fig. 2. Seismic transect on the topography/bathymetry map of the study area (Jakobsson *et al.* 2000). Red ticks with numbers show distance along transect in km. MD – Molloy Deep.

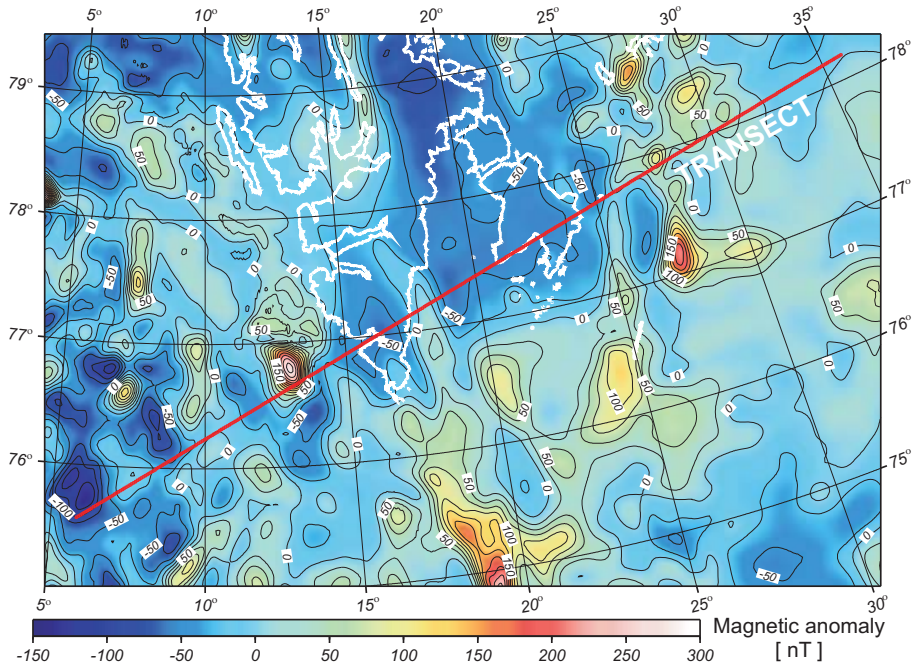

Fig. 3. Location of the seismic transect on the magnetic map of the study area (Maus *et al.* 2009).

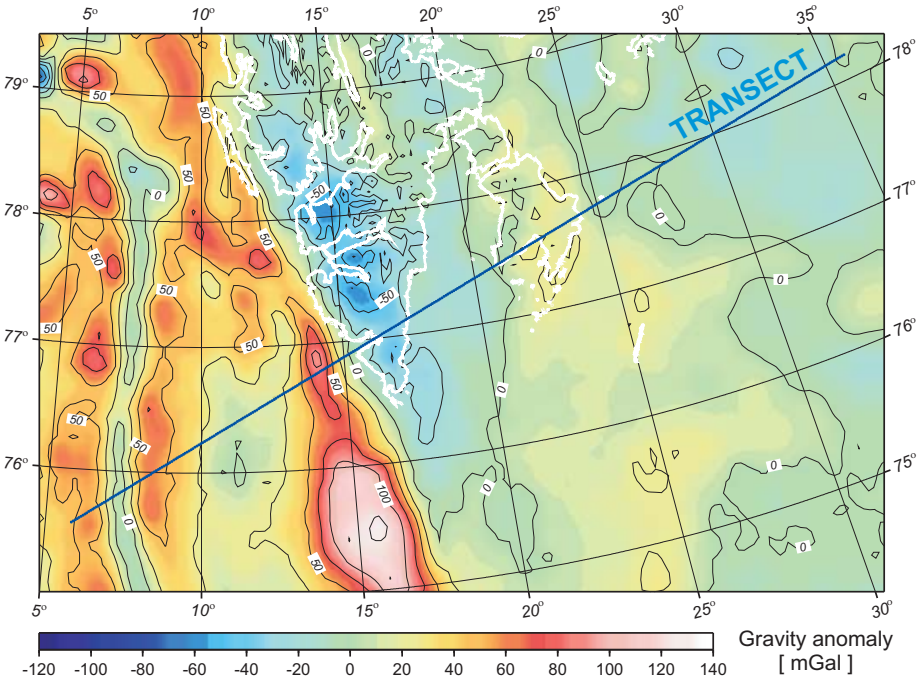

Fig. 4. Location of the seismic transect on the gravity map of the study area: free-air anomaly at sea and Bouguer on land with correction for density of 2.67 g/cm^3 (Kenyon *et al.* 2008).

the transect are: ϕ_0 = 75.573°N, λ_0 = 5.8316°E (0 km of transect, southwesternmost airgun shot) and ϕ_x = 78.1909°N, λ_x = 35.8286°E (800 km of transect, grey x in the northeasternmost end).

The acquisition of the data along the Profile 8 was performed in August 1998 using *R/V Håkon Mosby* (Ljones *et al.* 2004). Four Bolt 1500 C air guns with a total volume of 77.66 l were used as a seismic source. The shots were triggered by a Differential-GPS navigation system with one shot every 200 m. Ten analogue ocean bottom seismometers (OBS) were used to record the seismic data. Apart from refraction investigations a single-channel streamer, with a recording length of 6 s and sample rate of 1 ms, was used along the profile. Near-vertical reflection data were particularly effective in detailing the sedimentary structure.

Seismic investigations along the Horsted'05 profile were performed in August 2005 using *R/V Horyzont II* (Czuba *et al.* 2008). As a seismic sources three airguns with a total volume of 60 l and an average shot spacing of about 800 m were used, as well as 26 shots of 25–100 kg TNT charge, with an average spacing of about 5 km and 60 m depth. The seismic energy was recorded in-line by 11 land-stations deployed onshore and 10 OBSs.

Profile 8 and profile Horsted'05 overlap in the distance range 225–310 km. In general, good quality recordings at both profiles allowed a detailed study of the seismic wave field and crustal structure. Both models in the overlapping range were joined and re-modelled using ray tracing (SEIS83 software package; Červený *et al.* 1977; Červený and Pšenčík 1983). Examples of seismic record sections with re-calculated travel times for the joined transect are presented in Figs 5 and 6, together with ray diagrams.

A seismic refraction and reflection tomography experiment along Profile KKL (Minakov *et al.* 2012) was performed across the igneous province east of Svalbard. Seismic travel times from 12 OBSs and hydrophones deployed along a 170 km line were inverted to produce smooth 2D images of the crustal P-wave velocity and geometry of the acoustic basement and Moho. The crustal thickness is typical for continental shelf regions (30–34 km) and finger-shaped high-velocity anomalies (6.7–7.1 km/s) in the lower crust, reaching of 4–12% velocity perturbation, were obtained. Previously for this area similar Moho depths were reported in compilation of the 3D crustal model of the Barents Sea by Ritzmann *et al.* (2007), however, in their model the velocities in the lower crust were significantly higher (7.4–7.5 km/s). Because of this discrepancy we tested different velocity models in the distance range 500–800 km along the transect.

The range of Profile 8, Horsted'05 and KKL profiles together with data from 3D crustal model of the Barents Sea (velocity columnes; for location see blue pentagons in Fig. 1) are shown in Fig. 7 (Ljones *et al.* 2004; Czuba *et al.* 2008; Minakov *et al.* 2012; Ritzmann *et al.* 2007). The 2D seismic crustal model along the transect (Fig. 8) is complicated in the western part located near the Knipovich Ridge. Details of the sedimentary structure are well recognized by the near-verti-

cal reflection survey (Ljones *et al.* 2004). Sediments with P-wave velocity of 2.5–4.0 km/s reach the depth of up to 6 km. Below the sedimentary wedge the oceanic crust consists of three layers of 1–2 km thickness, with velocities of 4.5–5.5 km/s, about 6.7 km/s and about 7.3 km/s, respectively. The Moho depth increases from about 8 km near the Knipovich Ridge to about 13 km near the COB. A high velocity layer (6.7–7.1 km/s) with thickness up to 17 km is modelled in the lower crust east of the COB in the distance range 250–350 km. The Moho depth increases in this area to a maximum of about 33 km. The central part of the transect is rather simple, with an upper crustal layer with P-wave velocities in the range of 5.6–6.1 km/s, and a lower crustal layer characterized by P-wave velocities of 6.1–6.2 km/s. The maximum P-wave velocity is modelled at *c.* 6.3 km/s in the continental crust in the Storfjorden and Edgeøya area, where the Moho depth varies between 26 and 31 km. The eastern part of the transect (500–800 km) contains a lower crustal layer with velocities up to 7.1 km/s. In this area the Moho depth increases to a maximum of 36 km.

The P-wave velocity of the uppermost mantle, just below the Moho boundary, is generally 7.85–7.9 km/s in the oceanic part of the transect and 8.05–8.2 km/s in the continental part of the transect. The model of the deeper part of the mantle was built from 3D data (Levshin *et al.* 2007).

Magnetic and gravity data

Magnetic anomalies in the area of investigations are mostly from -100 to +50 nT (Fig. 3). Positive anomalies over +150 nT are observed west of Hornsund (76.8°N, 13.0°E), south of Sørkapp (75.0°N, 19.0°E) and in the Barents Sea west of Edgeøya (77.2°N, 27.5°E). They have all circular or elliptic shape with 50 to 100 km diameter. Another group of smaller anomalies occurs in the area of Kong Karls Land. The magnetic anomalies were sampled along the transect from grid of 2×2 arc min. A global Earth Magnetic Anomaly Grid (EMAG2) has been compiled from satellite, ship, and airborne magnetic measurements (Maus *et al.* 2009). EMAG2 is a significant update of the previous candidate grid for the World Digital Magnetic Anomaly Map. The resolution has been improved from 3 arc min to 2 arc min, and the altitude has been reduced from 5 to 4 km above the geoid. Additional grid and track line data have been included, both over land and the oceans. Wherever available, the original shipborne and airborne data were used instead of precompiled oceanic magnetic grids. Interpolation between sparse track lines in the oceans was improved by directional gridding and extrapolation, based on an oceanic crustal age model. The longest wavelengths (> 330 km) were replaced with the latest CHAMP satellite magnetic field model MF6. EMAG2 is available at http://geomag.org/models/EMAG2 and for permanent archive at http://earthref.org/cgi-bin/er.cgi?s=erda.cgi?n=970.

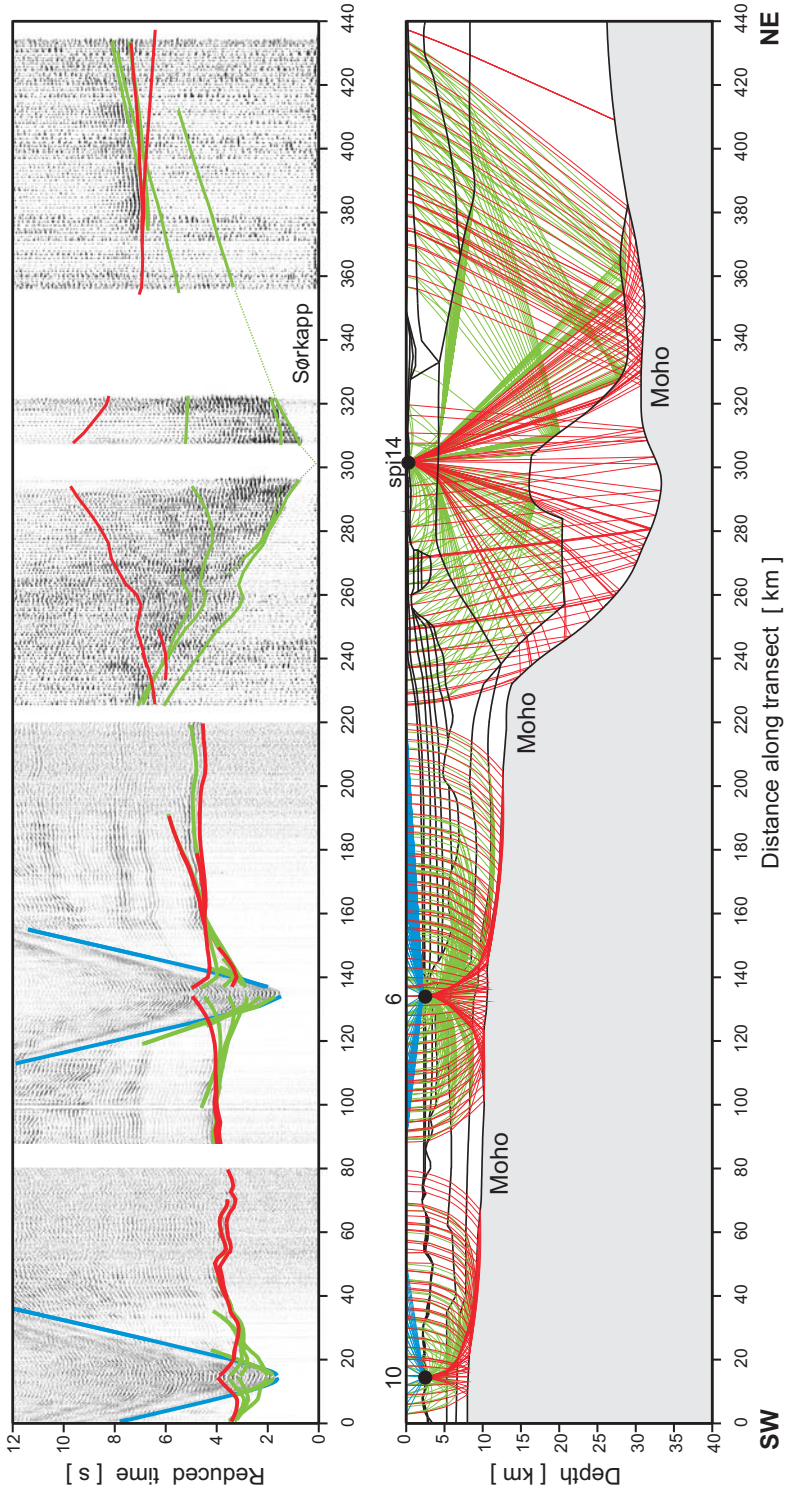

Fig. 5. Examples of amplitude-normalized seismic sections recorded along the eastern part of transect (receivers 10 and 6 at Profile 8 and station spi14 at profile Horsted'05). VA plots of normalized experimental record sections from airgun shots are shown with calculated traveltimes for the final model of the structure: blue lines – traveltimes of water waves, green lines – traveltimes of crustal phases, red lines – traveltimes of waves reflected and refracted from the Moho. In the bottom ray diagrams are shown with rays in colours corresponding to relevant traveltimes.

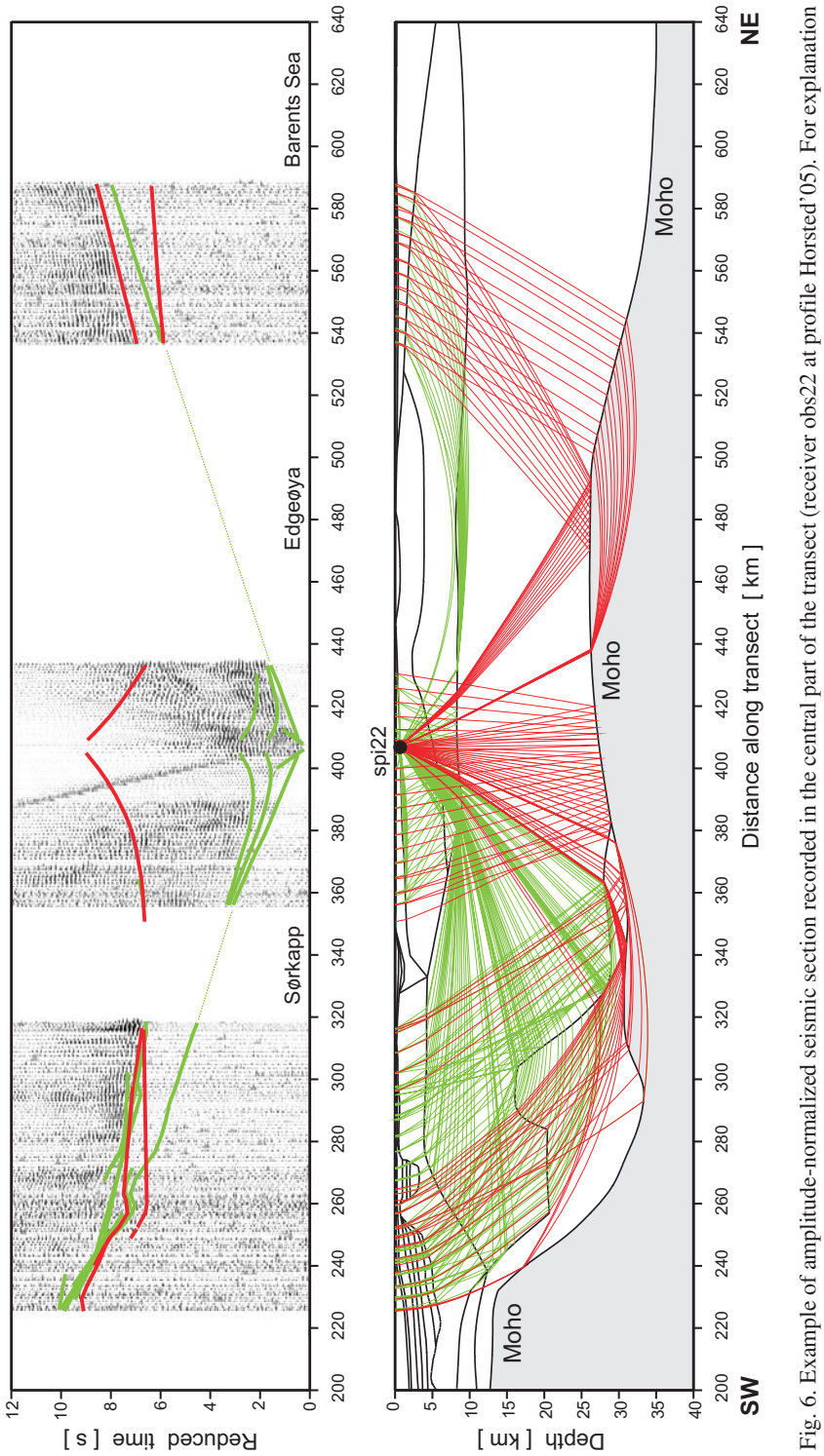

Fig. 6. Example of amplitude-normalized seismic section recorded in the central part of the transect (receiver obs22 at profile Horsted'05). For explanation see Fig. 5.

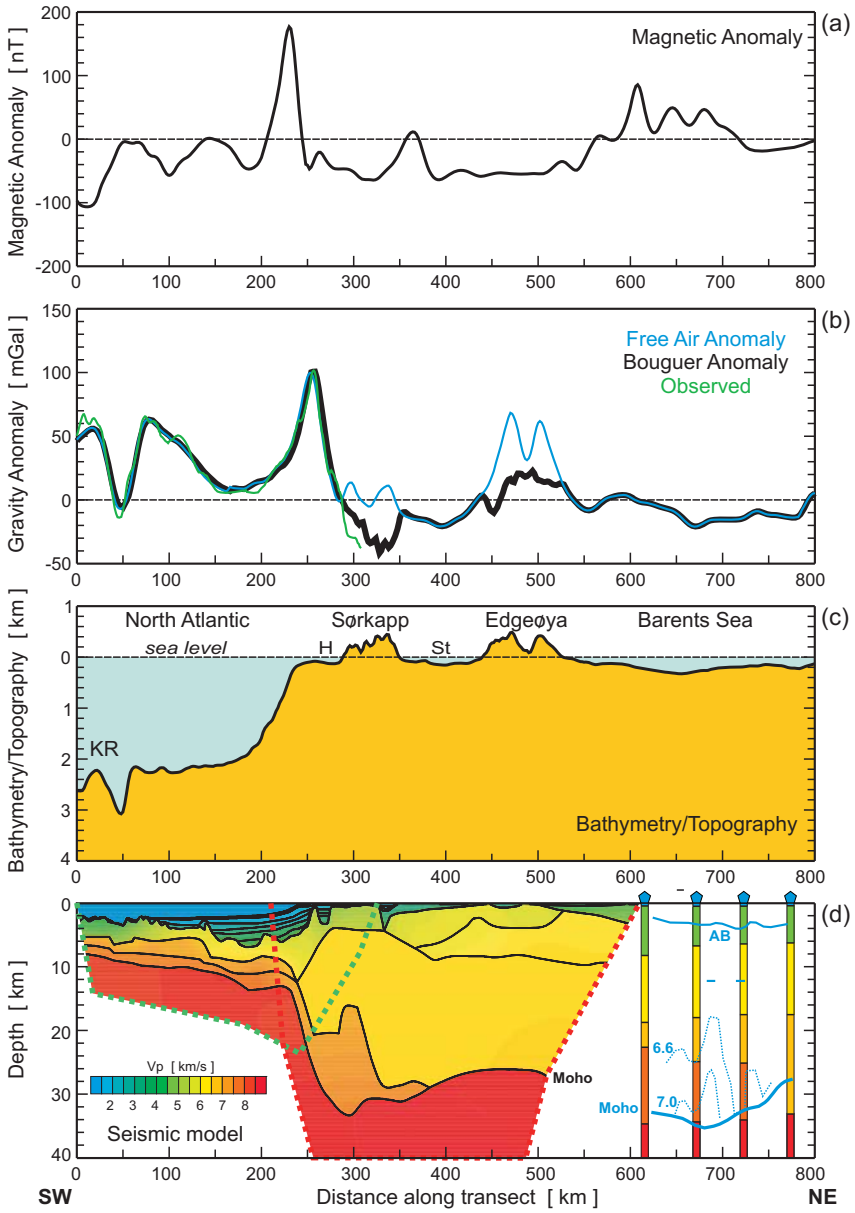

Fig. 7. Geophysical data along 2D transect. (a) Magnetic anomalies. (b) Gravity anomalies: free-air anomaly marked by blue line (Kenyon *et al.* 2008), Bouguer anomaly marked by thick black line (Kenyon *et al.* 2008), Bouguer anomaly measured along Profile 8 marked by green line (Ljones *et al.* 2004). (c) Bathymetry/topography (Jakobsson *et al.* 2000). (d) Crustal velocity model along the transect. Compilation from Profile 8 (limited by dotted green line frame; Ljones *et al.* 2004), profile Horsted'05 (limited by dotted red line frame; Czuba *et al.* 2008), Profile KKL (blue lines; Minakov *et al.* 2012) and from 3D crustal model of the Barents Sea (velocity columns beneath blue pentagons; Ritzmann *et al.* 2007). AB – acoustic basement; H – Hornsund; KR – Knipovich Ridge; St – Storfjorden; 6.6 and 7.0 – velocity isolines in km/s.

For gravity modelling the gravity map of the study area was compiled from free-air anomalies at the sea and Bouguer anomalies on the land (with correction for density of 2.67 g/cm^3) in grid of 5×10 min arc. Public domain gravity grids were derived from a multitude of sources of airborne, surface and submarine data in the Arctic (Kenyon *et al.* 2008). The data, prepared by a working group under the International Gravity and Geoid Commission, International Association of Geodesy, are available at http://earth-info.nga.mil/GandG/wgs84/agp/. As seen from the gravity map (Fig. 4) the transect runs nearly perpendicular to gravity anomalies, which is convenient for 2D modelling. Gravity anomalies were sampled from the maps every 2 km along the transect. Additionally, a LaCoste and Romberg sea gravity meter acquired gravity data along Profile 8 and Profile KKL (Fig. 8b).

Gravity modelling and its petrophysical consequences

Method. — The gravity modelling of the density cross-section related to the seismic model shown in Fig. 8 was performed using the optimisation concept (Krysiński *et al.* 2000; Krysiński 2009). The method postulates construction of some model density distribution $\rho(x, z)$ using a reference velocity-density relation $\rho_{ref}(v)$:

$$\rho_{ref}(V) := \begin{cases} 1.02\ \text{g/cm}^3 & \text{oceanic water} \\ 1.74\ [\text{g/cm}^3\ \text{km}^{-1/4}\text{s}^{1/4}]\cdot V^{1/4} & \text{for sediments} \\ 0.328\ [\text{g cm}^{-3}\ \text{km}^{-1}\text{s}]\cdot (V - 6\ \text{km/s}) + 2.723\ \text{g/cm}^3 & \text{in crystalline crust} \\ 3.3\ \text{g/cm}^3 & \text{mantle} \end{cases}$$

and corrections which can have separate form in every layer. The parameters defining these corrections are calculated to obtain the best fitting modelled gravity field to observed Bouguer anomalies, under the condition that the model density cannot differ from the reference value $\rho_{ref}(v(x, z))$ at any point of the cross section more than assumed density tolerance $\Delta\rho$. The value of the density tolerance should not be larger than 0.2 g/cm^3 but its exact value for the given case is estimated during modelling at the level above which significant improvement of gravity matching is not observed already. In this case the sufficient value of $\Delta\rho$ is 0.1 g/cm^3. The current modelling assumes space constant density correction γ_i of different value in every *i*-th layer in the crust and correction linearly dependent on local velocity $v(x, z)$ in the mantle $\alpha \cdot [v(x, z) - 8\ \text{km/s}] + \beta$ introducing two additional independent parameters α and β.

$$\rho(x,z) := \begin{cases} 1.02\ \text{g/cm}^3 & \text{oceanic water} \\ \rho_{ref}(v(x,z)) + \gamma_i & \text{crustal segments} \\ \rho_{ref}(v(x,z)) + \alpha \cdot v(x,z) + \beta & \text{mantle} \end{cases}$$

The water layer is treated separately due to its well determined density value 1.02 g/cm^3. Due to strong interdependence of the model parameters (γ_i, α and β) its determination is strongly instable and only some of them (*e.g.* α and β) can be well determined if they correspond to significant gravity response of recognizable shape. The use of the density tolerance of small value forces matching of other parameters at acceptable values near the reference line $\rho_{ref}(v)$. Because of the mentioned instability most of resulting density corrections values γ_i should not be interpreted and only the parameters γ_i, which have decisive tendency to be matched at the upper or lower limit of the allowed zone in the velocity-density diagram, are significant. Exceptionally, the model density in the mantle (*i.e.* parameters α and β) was not limited at all, because the modelling was aimed to study density features there. The stability of the mantle parameters determination seemed to be sufficient. The stability is a result of a clear shape of the model mantle gravity response (related to α and β), forced density calibration in the lower continental crust (3.0 to 3.2 g/cm^3) and not planar morphology of Moho and the mantle velocity field (Fig. 8). Taking into account shape of the mantle gravity field in the presented model one can expect that modelled mantle density values (3.15 g/cm^3) for smaller velocities 7.86 to 8 km/s correspond to uppermost oceanic mantle down to 30 km depth. This density is well determined in the modelling by its contrast to lower continental crust density which is approximately postulated by the $\rho_{ref}(v)$ function. However, the resulting mantle velocity-density correlation α correspond to the deeper mantle (40 to 150 km depth, Fig. 9) and it reflects general density difference between the oceanic and continental range. But the determined density in this deeper layer has no absolute calibration and we cannot be sure whether the value 3.2 g/cm^3 (for higher velocities) well represent uppermost continental mantle.

Usually the gravity modelling of a layered seismic model leads to difficulties, indicating that some density contrasts, not revealed by the seismic model, may exist along the profile. This problem is resolved by introduction of some approximately vertical density boundaries cutting the layers and defining a new block model (Fig. 10), with independent density corrections for each block. The number of boundaries, their positions and geometry are determined using a long procedure of trials and errors, which is primarily aimed at improvement of the gravity fitting (Krysiński *et al.* 2009b), but it is also to some degree tries to satisfy some tectonic requirements. The procedure uses simplified stratification of the crust (omitting subtle layering in the sedimentary section). Usually division into sediments and consolidated crust is sufficient for the purposes of gravity modelling, when vertical density boundaries are considered. The crystalline crust is divided by the density boundaries into parts called segments. Neglecting stratification in the consolidated crust is based on the observation that division of crustal segments into layers having independent density corrections leads (in this type of model) to artificial vertical density differences.

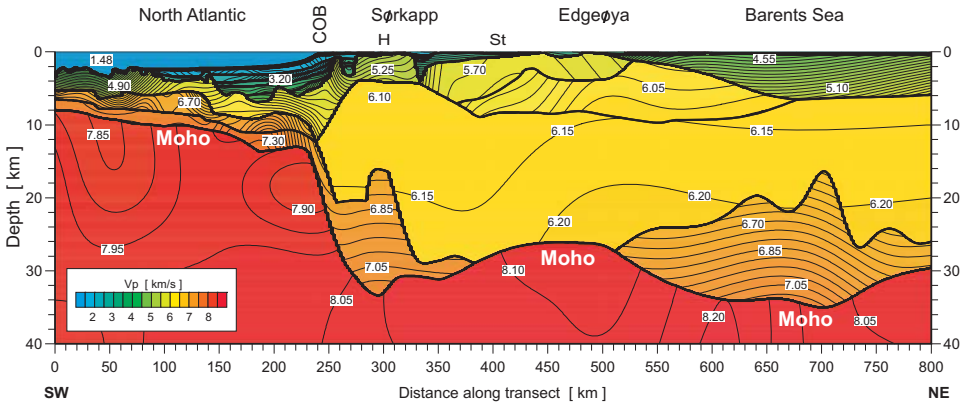

Fig. 8. Crustal two-dimensional seismic P-wave velocity model along the transect. In the distance range 0–500 km the model is based on Profile 8 (Ljones *et al.* 2004) and Horsted'05 (Czuba *et al.* 2008) and in the distance range 500–800 km the crustal model was constructed on the base of the 2D model along Profile KKL (Minakov *et al.* 2012). Mantle velocity model is taken from the 3D model of the Barents Sea (Levshin *et al.* 2007).

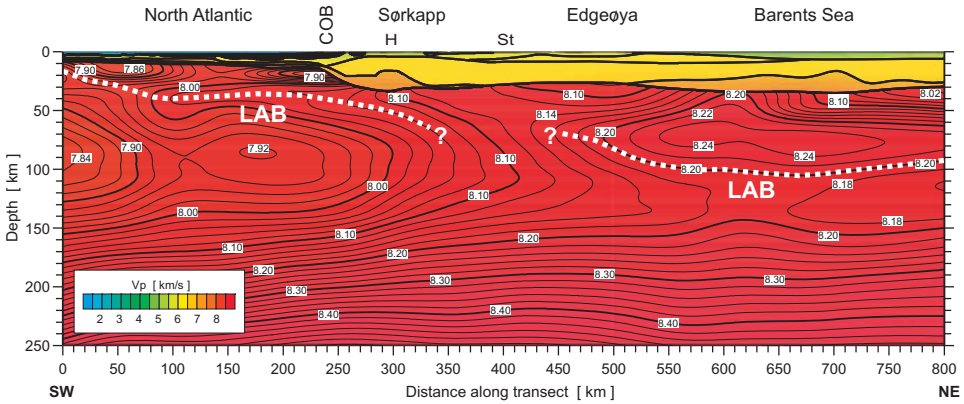

Fig. 9. Seismic P-wave velocity model down to 250 km compiled from the crustal model (see Fig. 8) and the mantle model (Levshin *et al.* 2007). The dashed lines show the lithosphere-asthenosphere boundary (LAB), close to the top of the low-velocity channel in the mantle. In the east it corresponds to velocity isoline 8.2 km/s at about 100 km depth. In the west it corresponds to velocity isoline 7.96 km/s at about 40 km depth, shallowing to *c.* 20 km below the Knipovich Ridge.

The divisional procedure and standard gravity modelling of the crust use a velocity model limited to shallow mantle depths (*e.g.* 40 km) and it applies a substitutive model of sub-crustal density distribution compensating the uneven crustal load according to the principle of isostasy (Krysiński *et al.* 2000; Krysiński 2009). This approach allows to estimate the characteristic depth position (here 70 to 90 km) of leading subcrustal horizontal density contrasts and the distribution along the profile, using analysis of the residual diagram (Krysiński 2009). At the beginning tests using standard modelling (without deeper mantle structure), both

the characteristic depth and horizontal distribution of the reconstructed compensation density structures turn out to be accordant with velocity model of the upper mantle below the profile (Fig. 9). The velocity model contain a thick layer of strong horizontal velocity variations (down to 150 km depth) with the same average depth of 80 km and general trend as the oceanic to continental change of the density of compensation masses. This similarity shows efficiency of the isostatic concept in reconstruction of the leading subcrustal density sources. But the accordance between the velocity field morphology and the predicted density compensation suggest the possibility of directly introducing the mantle velocity model into the gravity modelling instead of the substitutive model of compensation. The final model being presented here uses the mantle velocity distribution down to 180 km depth, below which the velocity distribution becomes flat and horizontal and this deeper part introduces nothing into the gravity modelling. In this model no additional density compensation was applied.

Density boundaries and crustal segments. — The divisional analysis (Krysiński *et al.* 2009b) provides strong constraints concerning the position and suggested declinations of the main density boundaries (A, B, C) along the profile (Fig. 10). A represents the COB, B is the eastern limit of the HFZ, C represents the eastern boundary of the West Spitsbergen Fold-and-Thrust Belt, and D intersects the crystalline basement at a major suture zone, corresponding to the Billefjorden Fault Zone at the surface. The other boundaries have less obvious links to geological features, but should be included in order to obtain a satisfactory gravity fit. Some of these weaker boundaries (D, E, F, α, β, γ, δ, ε, φ) may represent useful corrections of the seismic model or they can reflect offline (3D) effects.

The most significant density boundaries A and B along the profile represent the continent ocean boundary (COB) and the HFZ, respectively. The striking and very stably determined feature of this zone is its increased density in relation to the reference velocity-density function $\rho_{ref}(v)$ (Figs 11, 12 and 13; layer 10, gray). The decisive density excess can be recognised as its matching at the upper limit of the allowed density zone and keeping a high position while density tolerance $\Delta\rho$ become larger than 0.12 g/cm^3. The excess has large average value despite it was attributed to the whole crust within the transitional zone with steepest Moho gradient, but locally the real excess can have larger value. With respect to the small size (50 km wide) of the transitional zone and complexity of the velocity distribution morphology, some underestimation of seismic velocity (or imprecision of high velocity body shape leading to underestimation of high-velocity material volume) above the lower crustal body (LCB) can also be possible. Nevertheless, the properties of this layer (segment AB) have a specific position in the velocity-density diagram (Fig. 13, layer 10). This upper part of the allowed zone for crystalline crust in the velocity-density diagram, can correspond to mafic/ultramafic or high-grade metamorphic rocks (Gebrande 1982). The position might suggest that magmatic processes that occurred there during the final rift phase (break-up) led to increase

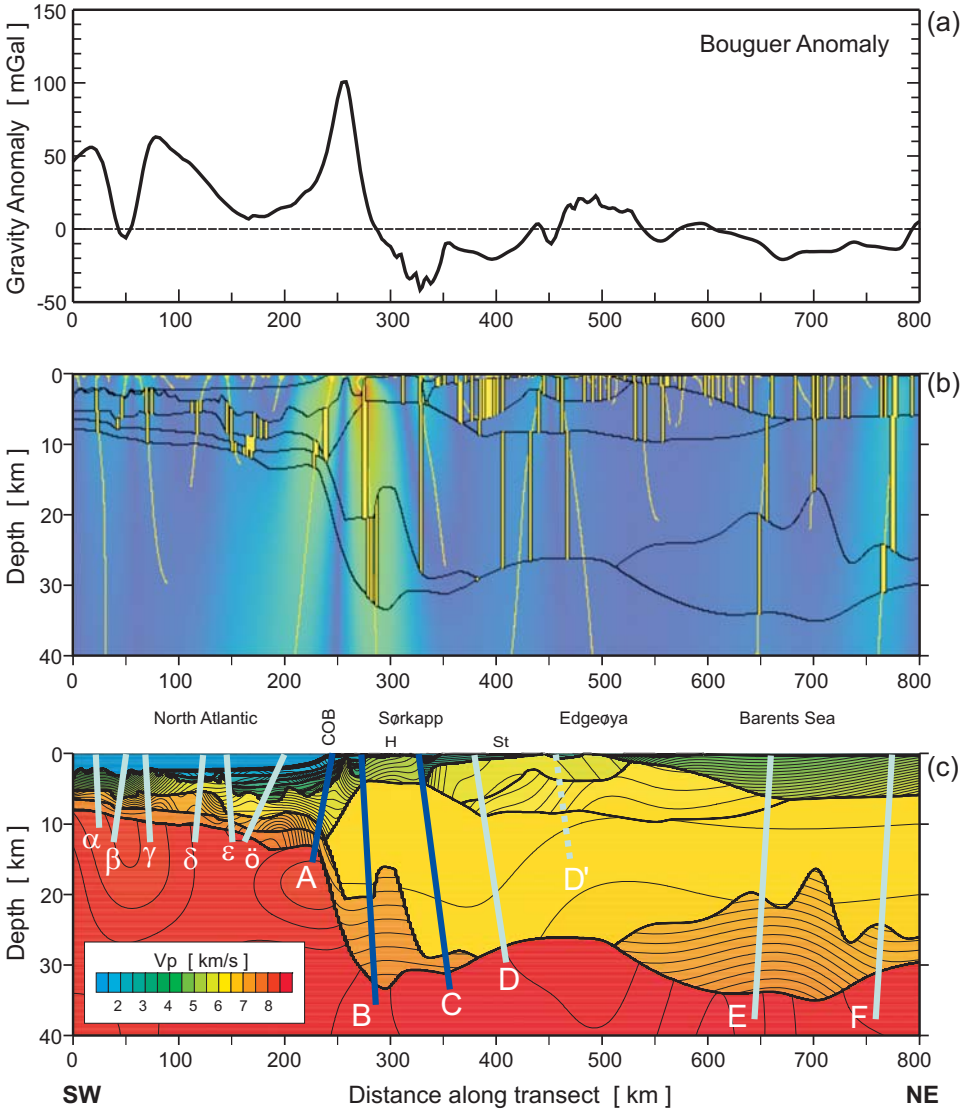

Fig. 10. The division of the crust into density blocks. (a) Bouguer anomaly. (b) Density boundaries with use of 120 divisions (Krysiński *et al.* 2009b); light colour intensity is proportional to efficiency of division. (c) The crustal model with six boundaries in oceanic segment (α, β, γ, δ, ε, φ), strong density boundaries (A, B, C), and weaker boundaries (D, D', E, F) in the continental crust.

of relative density, and that these processes are not limited to contamination of the continental crust by dense ultramafic material of Laurentian mantle or by material of lower crustal origin (high-velocity lower crust, LCB). In the case of such mixing the resulting material would have average properties (between standard crystalline crust and mantle properties) and average position in the velocity-density diagram, being situated below the central line $\rho_{ref}(v)$ (Fig. 13). In the neighbouring crustal

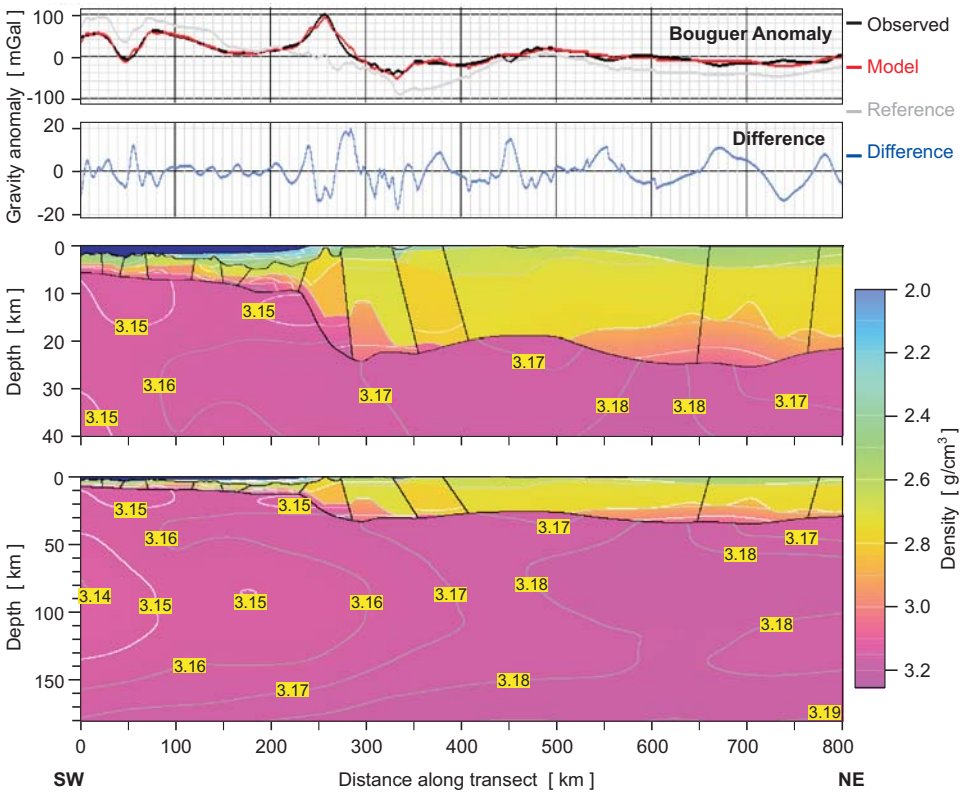

Fig. 11. The resulting density distribution $\rho(x, z)$ and modeled gravity field (red line) compared to observation (black line) and field related to velocity model converted to density using the assumed reference function $\rho_{ref}(v)$. The differences between model gravity field and observation are drawn as blue line. The resulting density distribution has small changes in the mantle and its subtle details are illustrated in Fig. 12.

segment, limited by boundaries B and C (West Spitsbergen Fold-and-Thrust Belt, WSFTB), a distinct deficiency of relative density was found. Some additional tests show that the density deficiency has generally upper-crustal position. This result might suggest that the upper-crustal the low-velocity massive (distance 275–330 km) has probably significantly deeper roots, deeper than than 5 km, as indicated in the seismic model.

Features of the mantle density. — The resulting dependence of the mantle density on local P-wave velocity 0.12 kg·s·m^{-4} denoted by α (Fig. 13), refers mostly to the horizontal velocity-density correlation because the possible vertical interdependence has no gravity response. In our case the resulting α value describes the general horizontal difference between oceanic and continental mantle in the layer between 40 and 150 km depth (Fig. 12).

These horizontal differences can be controlled by temperature or petrological differences (Romanyuk and Mooney 2007; Romanyuk *et al.* 2007). The determina-

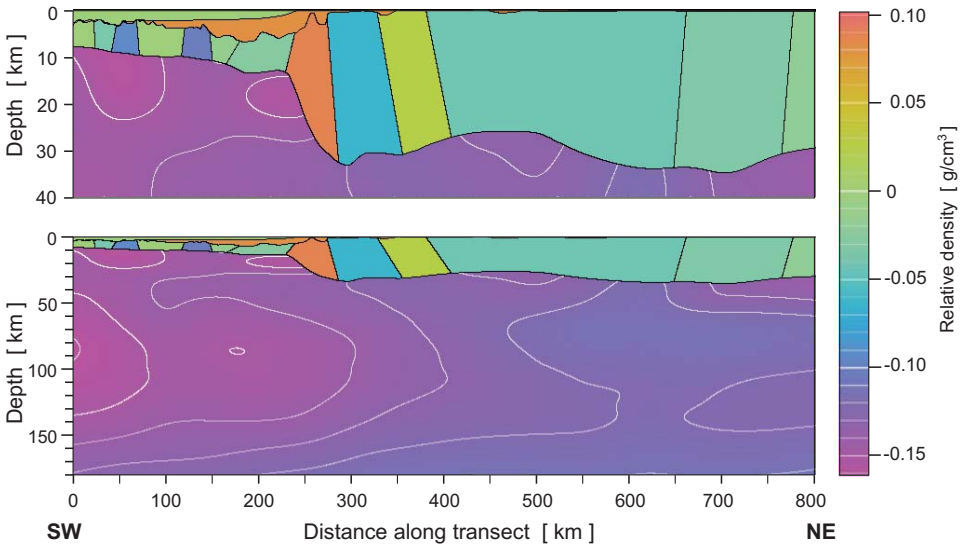

Fig. 12. The differences between the modeled density distribution $\rho(x, z)$ and reference density values $\rho_{ref}(v(x, z))$.

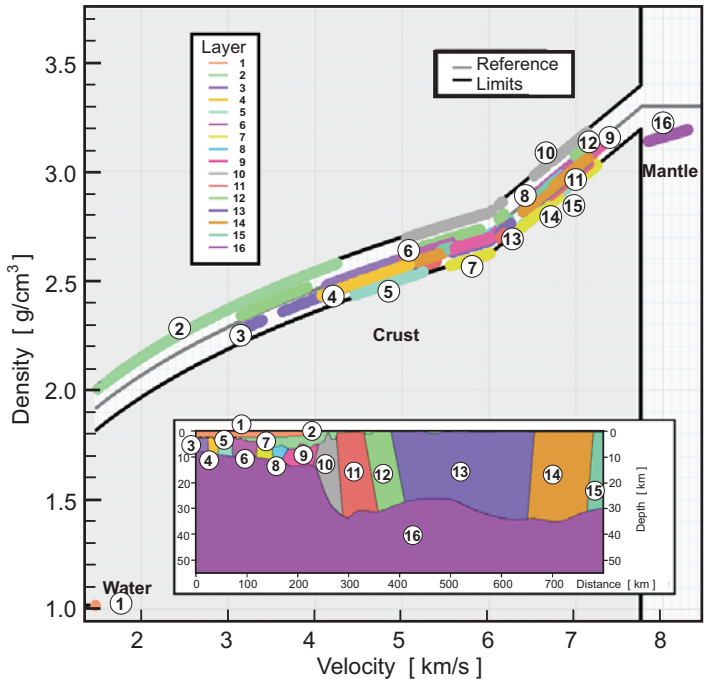

Fig. 13. Velocity-density diagram showing resulting dependences of density on velocity in every layer of the density model. The central line of the allowed zone (thin grey line) represents the reference relation $\rho_{ref}(v)$. The "forbidden" area is shaded in gray. The layer system is depicted in the insert. Note weak dependence of density on velocity in the mantle and relatively low mantle velocities.

tion and discussion of α on gravity grounds is possible when significant horizontal differences of velocity occurs along the profile, like in our case. The assumption that the effect has thermal nature would suggest that α would have a value of about 0.2 kg·s·m^{-4} ($\rho_m \cdot \gamma \cdot (\partial v/\partial T)^{-1}$ where mantle density $\rho_m \approx 3.3$ g/cm^3, volume thermal expansion coefficient $\gamma \approx 3.3 \cdot 10^{-5}$ K^{-1} (Parsons and Sclater 1977) and $\partial v/\partial T \approx -0.5 \cdot 10^{-3}$ km·s^{-1}·K^{-1} (Christensen and Mooney 1995). Mineral control for the correlation may provide values of α between 0 and 0.4 kg·s·m^{-4}, according to different concepts of dominant composition of the uppermost mantle and possible differences between continental and oceanic mantle. The larger values 0.3–0.4 kg·s·m^{-4} would correspond to oceanic and continental Precambrian crust (Birch 1964; Christensen and Mooney 1995, linear model), but so large value can be observed only in the uppermost mantle in the close vicinity of Moho when some mixing of mantle and crustal material occurs. Although eclogite is not preferred as an important component of the mantle in contemporary concepts, it should be noted that the α value corresponding to gabbro-eclogite transformation 0.4 kg·s·m^{-4} (Romanyuk *et al.* 2007) is also large. A weaker dependence (α between 0 and 0.1 kg·s·m^{-4}) with respect to changes of depletion degree is preferred in petrological studies for the asthenospheric and lithospheric mantle (Anderson and Bass 1984; Duffy and Anderson 1989; Jordan 1978, 1981; Sato *et al.* 1988, 1989; Sato and Sacks 1989).

Weak density dependence on velocity in the mantle is proposed by Christensen and Mooney (1995; alternative nonlinear model). Such flat behaviour of mantle density was noted earlier by Dortman *et al.* (1984; after Plewa and Plewa 1992) basing on a large number of continental samples well represented in the velocity-density diagram.

The discussion of the α value is not straightforward because due to the interplay of different types of phenomena controlling velocity-density correlation. The thermal anomalies are not necessarily correlated with compositional changes, thus the horizontal variations of the density possibly does not correlate perfectly witch velocity variations. Also depletion of peridotite is likely not the only compositional variation present in the mantle and one can expect different types of peridotites below younger continents (Phanerozoic), older continents (Precambrian) and ocean. In such case also rather small values of α are expected. Nevertheless, the results of the present gravity modelling ($\alpha \approx 0.12$ kg·s·m^{-4}; Fig. 13) suggest that the horizontal differences are dominated by mineralogical changes with participation of the thermal effect. The thermally controlled density changes can have comparable amplitude being better reflected in density than in the velocity field. Significant compositional differences are suggested by the large range of horizontal velocity variation, which has value about 0.4 km/s at 80 km depth level. This velocity change would correspond to about 800 K temperature differences in homogeneous mantle, which is not expected at this depth. Despite of interpretation difficulties, the resulting α has reasonable values, showing that gravity studies of the velocity-density correlation in the mantle are possible. In general, gravity mod-

elling using one long profile is not sufficient for providing stable results when major density features are studied. For better estimations one should use a larger amount of case studies in the given region, or a collection of profiles in joint modelling (Krysiński *et al.* 2009a).

The resulting values of the mantle density are low, having visible tendency to be comparable with the lower-crustal values. In the case of strongly varying Moho depth, the determination of the density in the uppermost mantle is strongly dependent on the density attributed to deepest continental crust. In this case, low mantle density is observed despite high densities in the lower continental crust were forced by the reference relation $\rho_{ref}(v)$. The resulting mantle density value (3.15 g/cm^3) corresponding to the lowest mantle velocities (7.86 to 8 km/s) refers to the uppermost young oceanic mantle (10 to 30 km depth). The highest density values 3.2 g/cm^3 would correspond to continental mantle, but the value is not certain because of lack of absolute density calibration at depths larger than 40 km (the deepest Moho). Nevertheless, the tendency toward low mantle density (less than 3.2 g/cm^3) is frequently observed in gravity modelling in Phanerozoic and uppermost Proterozoic areas like in Central and Western Europe, as opposed to Precambrian areas of the East European Craton (densities 3.3–3.4 g/cm^3), when it is based on estimates of the mantle density without prejudges defined by some reference function $\rho_{ref}(v)$ (Krysiński *et al.* 2009a).

Geological interpretations

In this section we will interpret the final geophysical transect in terms of rock types, ages and geodynamical evolution. Our geological and petrophysical interpretations of the profile are shown in Figs 14 and 15.

Oceanic crust and COB.— Oceanic crust formed at the Knipovich Ridge are found from the western end of the transect to the COB. The magmatic crust is overlain by a sedimentary cover up to 5 km thick. Roughly the uppermost half of this layer consists of glacial sediments deposited the last *c.* 2.5 Ma (Ljones *et al.* 2004), whereas the rest of the layer represents older Cenozoic sedimentary rocks. The thickness of the three layered magmatic crust varies between about 6 and 8 km. Similar variations have been observed elsewhere in the area, and is generally interpreted in terms of fluctuations between magmatic cells causing relatively thick crust, and amagmatic areas dominated by extension and to some extent serpentinisation of the upper mantle (Ljones *et al.* 2004).

The COB outlines the western boundary of the narrow, 40–50 km wide transition (distance 230–270 km) from clear oceanic crust (6.7–7.3 km/s, and densities relatively close to the reference values) to continental crust with significantly lower values (velocity *c.* 6.1 km/s, with density deficiency in WSFTB; Fig. 15). In the transitional zone a significant excess of density (of order 0.12 g/cm^3 in aver-

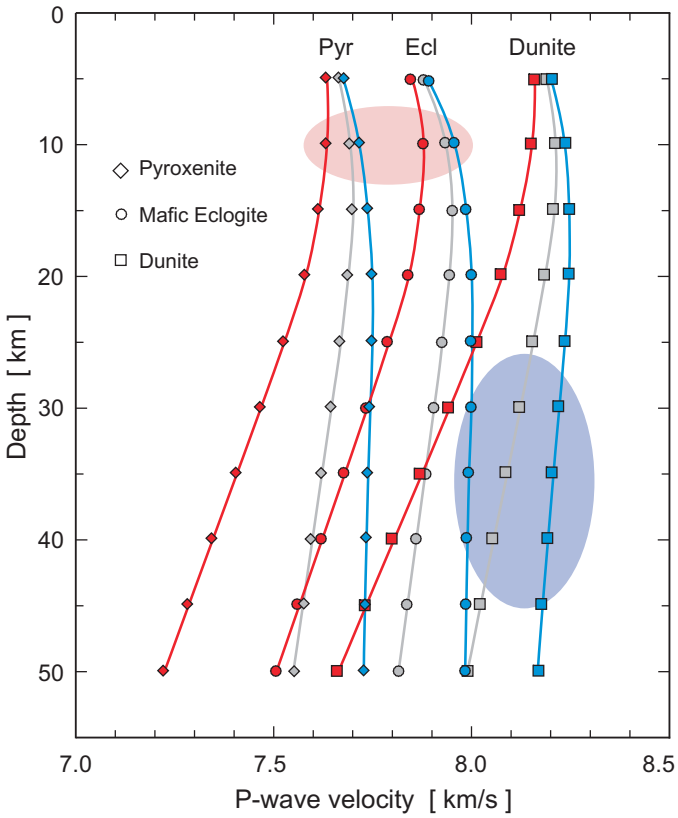

Fig. 14. P-wave velocity *versus* depth for pyroxenit, mafic eclogite and dunite for three heat flow regimes: high, average and low, marked in red, grey and blue, respectively (Christensen and Mooney 1995). Pink and blue areas show range of Vp velocities observed beneath the transect in the oceanic and continental uppermost mantle, respectively.

age) is observed in the crystalline crust, which suggests presence of mafic/ultramafic and metamorphic rocks. The margin is usually narrow in this region, dominantly affected by shear movements along Hornsund Fault Zone (Ljones *et al.* 2004), but our profile is also influenced by mafic intrusions indicating extension. Similar narrow transition has been documented further to the north (Ritzmann *et al.* 2003, 2004), and to the south (Breivik *et al.* 2003; Libak *et al.* 2012), along the same margin.

Sedimentary succession. — The COB marks the western boundary of the HFZ representing the system of strike-slip faults active during Early Cenozoic. The HFZ combined with later extension led to a system of grabens and horsts along the continental shelf. The West Spitsbergen Fold-and-Thrust Belt (WSFTB) is located immediately to the east of the HFZ. The WSFTB is a result of the Early Cenozoic trans-pressional movement along Spitsbergen, leading to the vertical strata that presently can be observed for example in the westernmost part of Van Mijenfjorden (*e.g.*

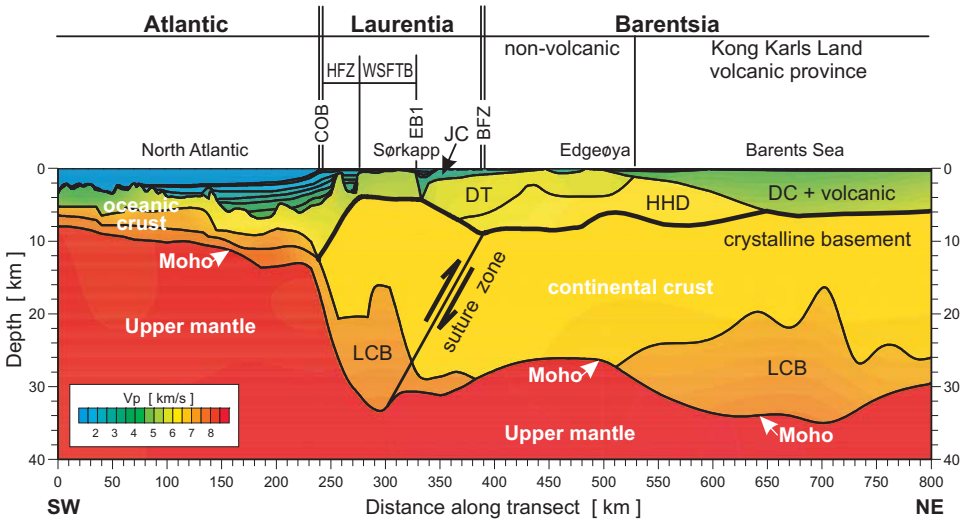

Fig. 15. Seismic P-wave velocity model along the transect with notification of geological units and tectonic interpretation of deeper structure. BFZ: Billefjorden Fault Zone (position of associated deep suture zone follows Breivik *et al.* 2003); COB – Continent-Ocean-Boundary; DT – Devonian–Triassic sedimentary unit; EB1 – eastern boundary of West Spitsbergen Fold-and-Thrust Belt (WSFTB); HFZ – Hornsund Fault Zone; HHD – Hecla Hoek basement, Devonian unit; JC – Jurassic–Cretaceous sedimentary unit.

Dallmann 1999). The strata within the WSFTB are of Silurian–Triassic age, and the zone is bounded to the east by the marked boundary EB1.

The uppermost layer between EB1 and Edgeøya is formed by Jurassic–Cretaceous (JC) sedimentary rocks. The velocities in this layer range from about 3.5 km/s to 5.0 km/s. The layer below (DT) expresses significantly higher velocities; 5.5–5.7 km/s and from exposures on Edgeøya it is known that its uppermost part consists of Triassic rocks. The deepest parts of the layer may consist of Devonian sedimentary rocks. This layer is underlain by a layer with velocities ranging from about 5.8 km/s to 6.0 km/s. We interpret this unit (HHD) as metamorphosed Hecla Hoek Basement representing Late Proterozoic to Silurian rocks (*e.g.* Dallmann 1999). It is possible that the uppermost part of the unit consists of Devonian sedimentary rocks. The uppermost layer east of Edgeøya expressing velocities in the range 4.5 km/s to 5.1 km/s, is interpreted as Devonian–Cretaceous (DC) deposits, mixed with Early Cretaceous volcanic rocks exposed immediately to the north at Kong Karls Land (KKLVP; Minakov *et al.* 2012). The relatively low velocities and velocities in this layer suggest that it dominantly consists of Cretaceous–Jurassic successions.

Continental crust and Caledonian suture. — Our interpretation of the top of the crystalline, continental crust follows the 6.1 km/s contour east of the COB. The continental crust can be divided in three areas: a western area with up to 29 km thick crust having general deficiency of density (in relation to the reference func-

tion $\rho_{ref}(v)$) located mostly at the upper part of the Laurentian crystalline crust and a high velocity layer (6.8–7.1 km/s) in the lower crust (LCB – lower crustal body), a central area with significantly thinner crust (18–21 km) and absence of a lower crustal high-velocity/density layer, and an eastern area with the same velocity characteristics as the western area, but relatively normal (close to reference function $\rho_{ref}(v)$) densities in contrast to the density anomalies within the HFZ and WSFTB zones (segment AB).

Along an OBS profile about 200 km south of our transect, Breivik *et al.* (2003) identified the main crystalline suture zone between the two lithospheric plates, Laurentia and Barentsia, active during the formation of the Caledonides. Primarily based on potential field data, they traced the suture zone northwards in Storfjorden and along Billefjorden, Spitsbergen (Breivik *et al.* 2005). Our transect seems to confirm this interpretation. The reverse fault (suture) as indicated in Fig. 15 has been subject to extensional reactivation, but the upper plate (Laurentia) thickened by stacking of thrust sheets is still at present significantly thicker than the lower plate. Following this interpretation, the HHD unit dominantly represents basement involved thrust sheets (nappes). The interpretation of the suture zone is furthermore supported by the down-to-the-west dipping crustal velocity iso-chrons, which was also observed by Breivik *et al.* (2003).

Due to its direct link with the volcanic rocks observed at Kong Karls Land, the LCB in the eastern part of the transect can most likely be related to magmatic intrusives. Minakov *et al.* (2012) linked the Early Cretaceous magmatism in this area to the generation of the Alpha Ridge, which Lawver and Muller (1994) related to the Siberian–Icelandic hotspot. The magmatism near Kong Karls Land appears to have been controlled by Paleozoic fault zones, and it was not accompanied by significant crustal thinning (Minakov *et al.* 2012). Assuming constant thickness of the main crustal layer for the Barentsia plate implies that about two-thirds of the LCB represents magmatic rocks emplaced in Early Cretaceous, the remaining part being older crustal rocks.

It is unlikely that the LCB located west of the suture zone can be related to the presence of serpentinized peridotites, as efficient fluid circulation would have been hampered by the > 15 km thick overlaying crust (Mjelde *et al.* 2003). The LCB may thus be interpreted in four different ways: (1) high-grade metamorphic rocks related to the formation of the Caledonides (Caledonian hypothesis); (2) emplacement of Early Cretaceous magmatic rocks (Cretaceous hypothesis); (3) magmatic rocks related to the Cenozoic continental break-up (Cenozoic hypothesis); (4) high-velocity lower crust of the Laurentian segment (of basically Precambrian age).

Breivik *et al.* (2003) found evidence for emplacement of high-grade metamorphic rocks, manifested as > 8 km/s rocks interpreted as eclogites formed during the continent-continent collision. It is possible to interpret the LCB in our transect as eclogites retrograded by fluids circulating during continent-continent collision. However, in this case we would have expected to observe the LCB also in the

Breivik *et al.* (2003) model. Its absence there leads to the conclusion that the Caledonian hypothesis is not very likely.

It can probably be excluded that the LCB represents break-up magmatism related to a mantle plume, since this ought to have led to higher velocities (7.2–7.5 km/s; Mjelde *et al.* 2008). Enhanced (normal temperature mantle) break-up magmatism may be caused by *e.g.* small-scale convection (Buck 1986), but if important in our case, such non-plume mechanisms ought to have been active along the entire margin segment. Since the LCB is observed landward of the COB further to the north (off northern Spitsbergen, Kongsfjorden and Van Mijenfjorden; Ritzmann *et al.* 2003, 2004; Czuba *et al.* 2005), but not further to the south (Breivik *et al.* 2003; Libak *et al.* 2012), we conclude that also the Cenozoic hypothesis is unlikely.

The LCB west of the suture zone has geophysical characteristics very similar to that of the Kong Karls Land LCB. Since the western LCB is observed for all available profiles north of our transect, we propose that the LCB is most likely related to Early Cretaceous magmatism channelled from the Arctic source southwards along the proto-Hornsund zone of weakness. The absence of the LCB along the Breivik *et al.* (2003) profile, suggests that the body terminates southwards around Sørkapp (Fig. 1).

The high-velocity LCB belongs to the Precambrian Laurentian segment of the profile. Such high-velocity lower crust is a typical feature of Precambrian crystalline crust, together with its larger thickness and three layered structure (*e.g.* Mooney *et al.* 1998; Grad *et al.* 2006). It is thus possible that the characteristics of the LCB west of the suture zone represent inherited, Laurentian processes.

Upper mantle. — The results of the gravity modelling show relatively weak correlation of the density with seismic velocity in the upper mantle $\alpha \approx 0.12$ kg·s·m^{-4}. The value suggests that the horizontal differences between oceanic and continental mantle are dominated (in terms of α value) by mineralogical changes like these caused by differences of depletion degree, but thermal effect is also present. The thermally controlled density changes can have comparable amplitude being better reflected in density than in the velocity field. Significant compositional differences are suggested also by large range of horizontal velocity variations.

The resulting values of the mantle density are generally low in comparison to some standard value 3.3 g/cm^3 represented by the reference function, and these low values refers to young uppermost mantle. Nevertheless, such low values are also noted in gravity modelling in continental areas of Phanerozoic age like in Central and Western Europe, strongly affected by young rift processes (*e.g.* Dérerová *et al*. 2006; Krysiński *et al*. 2009a).

The velocities and densities in the lithosperic upper mantle varies from minimum values of 7.85 km/s density 3.15 g/cm^3 beneath the oceanic crust to maximum values of 8.24 km/s density 3.2 g/cm^3 beneath the magmatic province in the eastern part of the transect (Fig. 14). The high values beneath the magmatic province may be interpreted in terms of low heat-flow and composition dominated by

dunites, an olivine-rich residue resulting from significant melting exhausting both clinopyroxene and orthopyroxene from the melt (Lee 2003). The lower values in the oceanic upper mantle lithosphere suggest composition dominated by primitive peridotites (lherzolithes) having experienced minor amounts of melt extraction. These peridotites contain significant amounts of clinopyroxene, orthopyroxene and plagioclase in addition to olivine.

This interpretation is supported by the observations and modelling of Christensen and Mooney (1995). P-wave velocity *versus* depth for three candidates for mantle material: pyroxenite, mafic eclogite and dunite are shown in Fig. 14. Following Christensen and Mooney (1995), velocity-depth relations are shown for three heat flow regimes: high, average and low, marked in red, grey and blue, respectively. Pink and blue areas show range of Vp velocities observed beneath the transect in the oceanic and continental uppermost mantle, respectively. This comparison suggests pyroxenite composition of the uppermost oceanic mantle, and dunite composition beneath continent.

Conclusions

The main part of the transitional zone between oceanic and continental crust, where the thickness of the crystalline crust increases systematically from about 7 to almost 30 km, is well imaged in the seismic model (at distance 230–270 km). The zone is limited by two distinctive boundaries (A and B), where large horizontal density contrasts occur in the crust. The crust within the transitional zone has significant excess of density (more than 0.1 g/cm^3 relative to the reference function) characteristic for mafic/ultramafic and high-grade metamorphic rocks, what suggests involvement of ultramafic material in magmatic processes during the rifting.

The velocity model of the upper mantle allows for successful direct description of subcrustal isostatic compensation, using assumption of approximately linear correlation between velocity and density. The estimated low value of correlation between density and velocity in the mantle 0.12 kg·s·m^{-4} suggests that horizontal density differences between oceanic and continental mantle would be dominated by compositional changes with some participation of thermal effects. The resulting α has reasonable value showing that gravity studies of the velocity-density correlation in the mantle are possible.

The velocities and densities in the lithosperic upper mantle varies from minimum values beneath the oceanic crust to maximum values beneath the magmatic province in the eastern part of the transect. The high values beneath the magmatic province may be interpreted in terms of low heat-flow and composition dominated by dunites. The lower values in the oceanic upper mantle lithosphere suggest composition dominated by primitive peridotites having experienced minor amounts of melt extraction.

Acknowledgements. — This work was partially supported by NCN grants UMO-2011/01/B/ST10/06653 and DEC-2011/02/A/ST10/00284. We acknowledge the Norwegian Petroleum Directorate, the Norwegian Research Council (NFR) and the Polish Oil and Gas Company S.A. (PGNiG) for funding seismic refraction experiments. The authors thanks Prof. Miroslav Bielik and Prof. Franjo Šumanovac for their valuable suggestions. The public domain GMT software (Wessel and Smith 1991, 1998) has been used for plotting maps.

References

ANDERSON D.L. and BASS J.D. 1984. Mineralogy and composition of the upper mantle. *Geophysical Research Letters* 11: 637–640.

BIRCH F. 1964. Density and composition of mantle and core. *Journal of Geophysical Research* 69 (20): 4377–4388.

BREIVIK A.J., VERHOEF J. and FALEIDE J.I. 1999. Effect of thermal contrasts on gravity modeling at passive margins: results from the western Barents Sea. *Journal of Geophysical Research* 104: 15,293–15,311.

BREIVIK A.J., MJELDE R., GROGAN P., SHIMAMURA H., MURAI Y. and NISHIMURA Y. 2003. Crustal structure and transform margin development south of Svalbard based on ocean bottom seismometer data. *Tectonophysics* 369: 37–70.

BREIVIK A.J., MJELDE R., GROGAN P., SHIMAMURA H., MURAI Y. and NISHIMURA Y. 2005. Caledonide development offshore-onshore Svalbard based on ocean bottom seismometer, conventional seismic, and potential field data. *Tectonophysics* 401: 79–117.

BUCK R.W. 1986. Small-scale convection induced by passive rifting; the cause for uplift of rift shoulders. *Earth and Planetary Science Letters* 77: 362–372.

ČERVENÝ V., MOLOTKOV I.A. and PŠENČÍK I. 1977. *Ray Method in Seismology*. Charles University, Prague: 214 pp.

ČERVENÝ V. and PŠENČÍK I. 1983. *2-D seismic ray tracing package SEIS83 (software package)*. Charles University, Prague.

CHRISTENSEN N.I. and MOONEY W.D. 1995. Seismic velocity structure and composition of the continental crust: A global view. *Journal of Geophysical Research* 100: 9761–9788.

CZUBA W., RITZMANN O., NISHIMURA Y., GRAD M., MJELDE R., GUTERCH A. and JOKAT W. 2005. Crustal structure of Northern Spitsbergen along deep seismic transect between the Molloy Deep and Nordaustlandet. *Geophysical Journal International* 161: 347–364.

CZUBA W., GRAD M., GUTERCH A., MAJDAŃSKI M., MALINOWSKI M., MJELDE R., MOSKALIK M., ŚRODA P., WILDE-PIÓRKO M. and NISHIMURA Y. 2008. Seismic crustal structure along the deep transect Horsted'05, Svalbard. *Polish Polar Research* 29 (3): 279–290.

DALLMANN W.K. (ed.) 1999. *Lithostratigraphic Lexicon of Svalbard*. Norwegian Polar Institute, Tromsø: 318 pp.

DAVYDOVA N.I., PAVLENKOVA N.I., TULINA Yu.V. and ZVEREV S.M. 1985. Crustal structure of the Barents Sea from seismic data. *Tectonophysics* 114: 213–231.

DÉREROVÁ J., ZEYEN H., BIELIK M. and SALMAN K. 2006. Application of integrated geophysical modeling for determination of the continental lithospheric thermal structure in the Eastern Carpathians. *Tectonics* 25: TC3009.

DORÉ A.G. 1991. The structural foundation and evolution of Mesozoic seaways between Europe and the Arctic. *Palaeogeography, Palaeoclimatology, Palaeoecology* 87: 441–492.

DORTMAN N.B. (ed.) 1984. *Physical properties of rocks and mineral deposits*. Nedra, Moscow: 455 pp. (in Russian).

DUFFY T.S. and ANDERSON D.L. 1989. Seismic velocities in mantle minerals and the mineralogy of upper mantle. *Journal of Geophysical Research* 94: 1895–1912.

ELDHOLM O., TSIKALAS F. and FALEIDE J.I. 2002. The continental margin off Norway 62–75°N: Palaeogene tectono-magmatic segmentation and sedimentation. *In*: D.W. Jolley and B.R. Bell (eds) The North Atlantic Igneous Province: Stratigraphy, Tectonics, Volcanic and Magmatic Processes. *Geological Society, London, Special Publications* 197: 39–68.

FALEIDE J.I., GUDLAUGSSON S.T., ELDHOLM O., MYHRE A.M. and JACKSON H.R. 1991. Deep seismic transects across the sheared western Barents Sea–Svalbard continental margin. *Tectonophysics* 189: 73–89.

FALEIDE J.I., VÅGNES E. and GUDLAUGSSON S.T. 1993. Late Mesozoic–Cenozoic evolution of the south-western Barents Sea in a regional rift-shear tectonic setting. *Marine and Petroleum Geology* 10: 186–214.

FALEIDE J.I., SOLHEIM A., FIEDLER A., HJELSTUEN B.O., ANDERSEN E.S. and VANNESTE K. 1996. Late Cenozoic evolution of the western Barents Sea–Svalbard continental margin. *Global and Planetary Change* 12: 53–74.

FALEIDE J.I., TSIKALAS F., BREIVIK A.J., MJELDE R., RITZMANN O., ENGEN Ø., WILSON J. and ELDHOLM O. 2008. Structure and evolution of the continental margin off Norway and the Barents Sea. *Episodes* 31 (1): 82–91.

GEBRANDE H. 1982. Elastic wave velocities and constants of elasticity of rocks and rock forming minerals. *In*: G. Angenheister (ed.) *Landolt-Börnstein, Physical Properties of Rocks, Band V/1b*. Springer Verlag, Berlin, Heidelberg: 1–99.

GRAD M., JANIK T., GUTERCH A., ŚRODA P., CZUBA W. and EUROBRIDGE'94–97, POLONAISE'97 and CELEBRATION 2000 SEISMIC WORKING GROUPS 2006. Lithospheric structure of the western part of the East European Craton investigated by deep seismic profiles. *Geological Quarterly* 50 (1): 9–22.

JACKSON H.R., FALEIDE J.I. and ELDHOLM O. 1990. Crustal structure of the sheared southwestern Barents Sea continental margin. *Marine Geology* 93: 119–146.

JAKOBSSON M., CHERKIS N.Z., WOODWARD J., MACNAB R. and COAKLEY B. 2000. New grid of Arctic bathymetry aids scientists and mapmakers. *EOS, Transaction, American Geophysical Union* 81 (9): 89, 93, 96.

JORDAN T.H. 1978. Composition and development of the continental tectosphere. *Nature* 274: 544–548.

JORDAN T.H. 1981. Continents as a Chemical Boundary Layer. *Philosophical Transactions of the Royal Society London* 301: 359–373.

KENYON S., FORSBERG R. and COAKLEY B. 2008. New Gravity Field for the Arctic. *EOS, Transaction, American Geophysical Union* 89 (32): 289.

KLINGELHÖFER F., GÉLI L. and WHITE R.S. 2000a. Geophysical and geochemical constraints on crustal accretion at the very-slow spreading Mohns Ridge. *Geophysical Research Letters* 27 (10): 1547–1550.

KLINGELHÖFER F., GÉLI L., MATIAS L., STEINSLAND N. and MOHR J. 2000b. Crustal structure of a super-slow spreading centre: a seismic refraction study of Mohns Ridge, 72°N. *Geophysical Journal International* 141: 509–526.

KRYSIŃSKI L., GRAD M. and POLONAISE WORKING GROUP 2000. POLONAISE'97-Seismic and gravimetric modelling of the crustal structure in the Polish basin. *Physics and Chemistry of the Earth, Part A* 25: 355–363.

KRYSIŃSKI L. 2009. Systematic methodology for velocity-dependent gravity modelling of density crustal cross-sections, using an optimization procedure. *Pure and Applied Geophysics* 166: 375–408.

KRYSIŃSKI L., GRAD M. and WYBRANIEC S. 2009a. Searching for regional crustal velocity-density relations with the use of 2-D gravity modelling – Central Europe case. *Pure and Applied Geophysics* 166: 1913–1936.

KRYSIŃSKI L., GRAD M. and WYBRANIEC S. 2009b. 2-D gravity modelling as a method of searching for deep-seated horizontal density contrasts in the Earth's crust. *Geophysical Research Abstracts* 11:

EGU2009-3141, EGU Gen. Ass. 2009, 19–24 April, 2009 Vienna, Austria http://meetings.copernicus.org/egu2009, p. 3141.

LAWVER L.A. and MÜLLER R.D. 1994. Iceland Hotspot track. *Geology* 22: 311–314.

LEE C.-T.A. 2003. Compositional variation of density and seismic velocities in natural peridotites at STP conditions: Implications for seismic imaging of compositional heterogeneities in the upper mantle. *Journal of Geophysical Research* 108 (9): 6–20.

LEVSHIN A.L., SCHWEITZER J., WEIDLE C., SHAPIRO N.M. and RITZWOLLER M.H. 2007. Surface wave tomography of the Barents Sea and surrounding regions. *Geophysical Journal International* 170: 441–459.

LIBAK A., EIDE C.H., MJELDE R., KEERS H. and FLÜH E.R. 2012. From pull-apart basins to ultraslow spreading: Results from the western Barents Sea Margin. *Tectonophysics* 514–517: 44–61.

LJONES F., KUWANO A., MJELDE R., BREIVIK A., SHIMAMURA H., MURAI Y. and NISHIMURA Y. 2004. Crustal transect from the North Atlantic Knipovich Ridge to the Svalbard Margin west of Hornsund. *Tectonophysics* 378: 17–41.

LYBERIS N. and MANBY G. 1993a. The origin of the West Spitsbergen Fold Belt from geological constraints and plate kinematics: implications for the Arctic. *Tectonophysics* 224: 371–391.

LYBERIS N. and MANBY G. 1993b. The West Spitsbergen Fold Belt: the result of Late Cretaceous–Palaeocene Greenland-Svalbard Convergence? *Geological Journal* 28: 125–136.

MAUS S., BARCKHAUSEN U., BERKENBOSCH H., BOURNAS N., BROZENA J., CHILDERS V., DOSTALER F., FAIRHEAD J.D., FINN C., VON FRESE R.R.B., GAINA C., GOLYNSKY S., KUCKS R., LUHR H., MILLIGAN P., MOGREN S., MULLER D., OLESEN O., PILKINGTON M., SALTUS R., SCHRECKENBERGER B., THEBAULT E. and CARATORI TONTINI F. 2009. EMAG2: A 2-arc-minute resolution Earth Magnetic Anomaly Grid compiled from satellite, airborne and marine magnetic measurements. *Geochemistry, Geophysics, Geosystem* 10: Q08005.

MINAKOV A., MJELDE R., FALEIDE J.I., FLUEH E.R., DANNOWSKI A. and KEERS H. 2012. Mafic intrusions east of Svalbard imaged by active-source seismic tomography. *Tectonophysics* 518–521: 106–118.

MJELDE R., BREIVIK A.J., ELSTAD H., RYSETH A.E., SKILBREI J.R., OPSAL J.G., SHIMAMURA H., MURAI Y. and NISHIMURA Y. 2002. Geological development of the Sørvestsnaget Basin, SW Barents Sea, from ocean bottom seismic, surface seismic and potential field data. *Norwegian Journal of Geology* 82: 183–202.

MJELDE R., KASAHARA J., SHIMAMURA H., KAMIMURA A., KANAZAWA T., KODAIRA S., RAUM T. and SHIOBARA H. 2003. Lower crustal seismic velocity-anomalies: magmatic underplating or serpentinized peridotite? Evidence from the Vøring Margin, NE Atlantic. *Marine Geophysical Research* 23: 169–183.

MJELDE R., BREIVIK A.J., RAUM T., MITTELSTAEDT E., ITO G. and FALEIDE J.I. 2008. Magmatic and tectonic evolution of the North Atlantic. *Journal of Geological Society* 165: 31–42.

MOONEY W.D., LASKE G. and MASTERS T.G. 1998. CRUST 5.1: A global crustal model at 5°×5°. *Journal of Geophysical Research* 103: 727–747.

OHTA Y. 1994. Caledonian and Precambrian history in Svalbard: a review, and an implication of escape tectonics. *Tectonophysics* 231: 183–194.

PARSONS B. and SCLATER J.G. 1977. An analysis of the variation of ocean floor bathymetry and heat flow with age. *Journal of Geophysical Research* 182: 803–827.

PLEWA M. and PLEWA S. 1992. *Petrophysics*. Wydawnictwa Geologiczne, Warszawa: 327 pp. (in Polish).

RIIS F., LUNDSCHIEN B.A., HØY T., MØRK A. and MØRK M.B.E. 2008. Evolution of the Triassic shelf in the northern Barents Sea region. *Polar Research* 27: 318–338.

RITZMANN O., JOKAT W., MJELDE R. and SHIMAMURA H. 2003. Crustal structure between the Knipovich Ridge and the Van Mijenfjorden (Svalbard). *Marine Geophysical Research* 23: 379–401.

RITZMANN O., JOKAT W., CZUBA W., GUTERCH A., MJELDE R. and NISHIMURA Y. 2004. A deep transect from Hovgård Ridge to northwestern Svalbard across the continental-ocean transition: A sheared margin study. *Geophysical Journal International* 157: 638–702.

RITZMANN O., MAERCKLIN N., FALEIDE J.I., BUNGUM H., MOONEY W.D. and DETWEILER S. 2007. A three-dimensional geophysical model of the crust in the Barents Sea region: model construction and basement characterization. *Geophysical Journal International* 170: 417–435.

ROMANYUK T. and MOONEY W.D. 2007. Seismic P-wave velocities – density relation in the upper mantle of the Western USA. *Geophysical Research Abstracts* Vol. 9, 00822, SRef-ID:1607-7962/gra/EGU2007-A-00822.

ROMANYUK T., MOONEY W.D. and DETWEILER S. 2007. Two lithospheric profiles across southern California derived from gravity and seismic data. *Journal of Geodynamics* 43: 274–307.

SATO H. and SACKS I.S. 1989. Anelasticity and thermal structure of the oceanic mantle: Temperature calibration with heat flow data. *Journal of Geophysical Research* 94 (5): 5705–5715.

SATO H., SACKS I.S., TAKAHASHI E. and SCARFE C.M. 1988. Geotherms in the Pacific Ocean from laboratory and seismic attenuation studies. *Nature* 336: 154–156.

SATO H., SACKS I.S., MURASE T., MUNCILL G. and FUNKUYAMA H. 1989. Qp-melting temperature relation in peridotite at high pressure and temperature: Attenuation mechanism and implications for the mechanical properties of the upper mantle. *Journal of Geophysical Research* 94 (8): 10647–10661.

SELLEVOLL M.A. (coordinator) 1982. *Seismic crustal studies on Spitsbergen 1978*. Geophysical Research on Spitsbergen, Bergen: 62 pp.

SUNDVOR E. and ELDHOLM O. 1979. The western and northern margin off Svalbard. *Tectonophysics* 59: 239–250.

SUNDVOR E. and ELDHOLM O. 1980. The continental margin of the Norwegian-Greenland Sea: Recent and outstanding problems. *Transactions of the Royal Society of London Series A* 294: 77–82.

TAYLOR P.T., KOVACS L.C., VOGT P.R. and JOHNSON G.L. 1981. Detailed aeromagnetic investigation of the Arctic Basin, 2. *Journal of Geophysical Research* 86 (B7): 6323–6333.

VOGT P.R., TAYLOR P.T., KOVACS L.C. and JOHNSON G.L. 1979. Detailed aeromagnetic investigation of the Arctic Basin. *Journal of Geophysical Research* 84: 1071–1089.

WESSEL P. and SMITH W.H.F. 1991. Free software helps map and display data. *EOS, Transaction, American Geophysical Union* 72 (41): 445–446.

WESSEL P. and SMITH W.H.F. 1998. New, improved version of Generic Mapping Tools released. *EOS, Transaction, American Geophysical Union* 79 (47): 579.

WORSLEY D. 2008. The post-Caledonian development of Svalbard and the western Barents Sea. *Polar Research* 27: 298–317.

Received 5 February 2013
Accepted 22 April 2013